International Journal of Heat and Mass Transfer 52 (2009) 4664–4668

Contents lists available at ScienceDirect

International Journal of Heat and Mass Transfer

journal homepage: www.elsevier.com/locate/ijhmt

Technical Note

Saturation evolution induced by inner pore structural effects in a porous material during wetting

D. Wu, X.F. Peng *

Laboratory of Phasechange and Interfacial Transport Phenomena, Department of Thermal Engineering, Tsinghua University, Beijing 100084, China

ARTICLE INFO

Article history:
Received 19 July 2008
Received in revised form 16 March 2009
Accepted 23 March 2009
Available online 6 May 2009

Keywords:
Saturation
Porous media
Micro CT
Wetting

ABSTRACT

A series of experiments was conducted to observe the transport phenomena in wood during wetting using a micro CT (scanning analysis technology). Both saturation evolution and corresponding liquid transfer are nondestructively investigated for both pendular and funicular mode at pore structure level in porous media. A method was proposed to obtain the important real inner structure information of porous media, as well as saturation profile and evolution, and corresponding liquid migration. From experimental observations, the pendular and funicular mode could be identified distinctly, and their transport behavior induced by inner structural effects was explored based on local pore structural information. And particularly, the dynamical saturation evolution and corresponding existence of distinct accumulation states were further discussed for the pendular mode.

1. Introduction

Fluid wetting (imbibition) in a porous medium is the process by which a nonwetting fluid, such as oil or air, is displaced by the spontaneous entry of a wetting fluid, such as water or brine, by means of capillary action. Nowadays, more and more attention is paid to conducting comprehensive investigations on transport phenomena in various porous media during wetting, since they widely exist and play critically important roles in natural world and practical applications, such as oil recovery, food industry, soil science, irrigation in agriculture, and wetting of raw material powders in industrial chemistry. Inspired by this tremendous practical importance, many experiments were conducted in search of a thorough physical understanding of the basic mechanisms involved, such as wetting rate and front movement [1–3]. Theoretical models have also been developed over long periods in different fields [4–6]. It is found that liquid saturation evolution characteristics and corresponding accumulation states inside complex pore structure are reasonably expected to intensely influence on wetting behaviors of various practical processes and performance of industrial systems/devices, especially for mini/micro pore structures.

In unsaturated porous media, liquid often exists or is distinguished in two different modes of existence, or "funicular" and "pendular" mode. Irreducible saturation at which $S = S_{irr}$ was introduced to identify these two modes [7]. For funicular mode ($S \geqslant S_{irr}$), free liquid remains continuous and bulk flow exists in pore structures. For funicular mode, pore network model can be utilized to discuss wetting behaviors [8,9]. However, one major limitation of applying network models is the ability to fully capture pore-scale characteristics of a network model according to actual pore structure. For pendular mode ($0 \leqslant S \leqslant S_{irr}$), liquid accumulates discontinuously and no bulk liquid flow exists in pore structures. Different theoretical models were developed to describe liquid transfer in this mode [10,11], and some improvements were made [12,13]. However, there is still a lack to justify the assumptions in these models. It is obviously very essential to investigate actual water accumulation states, whether liquid film exists or not, and corresponding transport behavior.

So far, CT-scanner and corresponding three-dimensional tomography allows researchers to nondestructively image porous media systems with high-resolution [14,15]. In present work, a micro-CT scanner was utilized to nondestructively portray the dynamical transport behavior during wetting. Saturation evolution and corresponding liquid transfer for both funicular and pendular mode are investigated at pore structure level in real porous media during spontaneous wetting processes. For each mode transport behavior induced by inner structural effects was explored based on local pore structural information. Particularly, for the pendular mode, existence of distinct accumulation states, such as assembling in a narrow slit, droplet or film on a pore wall surface, as well as their dynamical evolution during wetting, were further discussed based on the experimental observations.

2. Experiments

The experimental facility was mainly a portable micro-CT scanner SKYSCAN 1074 made in Belgium to nondestructively portray

* Corresponding author. Tel./fax: +86 10 6278 9751.
E-mail address: pxf-dte@mail.tsinghua.edu.cn (X.F. Peng).

0017-9310/$ - see front matter © 2009 Elsevier Ltd. All rights reserved.
doi:10.1016/j.ijheatmasstransfer.2009.03.035

Nomenclature

GS	grey scale
S	saturation
S_{irr}	irreducible saturation

Greek symbols

ε	porosity
ρ	density of the sample (kg/m^3)

Subscripts

0	before scanning
1	after scanning
a	air
s	solid of porous (wood tissue)
w	water liquid

the inner information of the test samples, including matter density as well as inner structure, pore size distribution and other associated information with/without water inside the samples. The reconstructed cross-section image scales have a maximum size of 732×732 pixels with 256 grey scales, and each pixel size is 37.6×37.6 μm. Both principle and associate experimental technology of the micro-CT scanner were described in the previous work [16].

Cylinder wood samples served as the porous media in this investigation with a diameter of 9.5 mm and a length of 25 mm. Before wetting experiments, each dry wood sample was first scanned by the micro-CT Scanner to attain real inner pore structure information as a critical reference of future experimental data reductions and phenomenon observations, particularly water state and migration in the wood sample. Fig. 1(a) depicts a longitudinal shadow image of the dry erected cylinder wood sample scanned directly by X-ray from one direction. A great number of shadow images similar to that shown in Fig. 1(a) were assembled to reconstruct a cross section shown in Fig. 1(b) at a specified location.

Another critical issue for the processing and analysis of experimental results is to accurately determine/choose referring positions and/or bases of result analysis and comparison. Line 1 in Fig. 1(a) shows the location of a scar cut on wood sample to ensure images of the same cross-section reconstructed. To further explore the difference of inner information during wetting clearly and comparably, a referring line was drawn starting from the specified center point (position O) normal to the straight outside edge (position A) in Fig. 1(b). In the followings the experimental results are discussed at this line of a specified cross-section.

In the experiments, each wood sample was fully put into water to get wetted spontaneously and taken to scan after wetted 4, 8 and 32 h, respectively. Cross-section images of different wetting stages were obtained. Porosity and saturation can be obtained as [17].

$$\varepsilon = \frac{GS_0 - GS_s}{GS_a - GS_s} \tag{1}$$

$$S = \frac{(GS_1 - GS_0)(GS_a - GS_s)}{(GS_0 - GS_s)(GS_w - GS_a)} \tag{2}$$

where, GS_0 and GS_1 are the grey scales of a single pixel of the dry wood without water and wetted wood containing some water, respectively. GS_a, GS_w and GS_s represent the grey scales of pure air, water and solid wood, respectively, with the value of $GS_s = 105$ and $GS_w = 90$. GS_a can be derived from

$$GS_a = \frac{\rho_w - \rho_a}{\rho_w - \rho_s}(GS_s - GS_w) + GS_w. \tag{3}$$

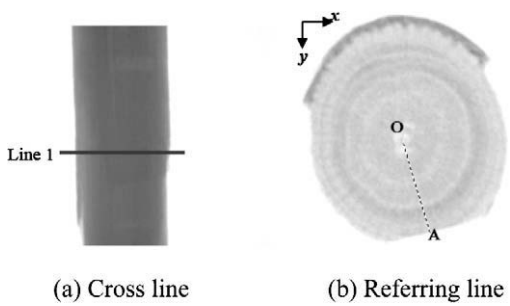

Fig. 1. Scanned image.

3. Wetting characteristics

3.1. Porosity distribution

Fig. 2(a) and (b) illustrate the calculated results of the porosity using Eq. (1) and the histogram of porosity distribution, respectively, corresponding to the image in Fig. 1(b). In Fig. 2(b), there are two peaks of pixels obviously existing at two porosities corresponding to 0.55 and 1.0, respectively. The pixels at the porosity value of 1.0 were mainly contributed by the air region in Fig. 1(b). Setting 0.95 as the threshold value to separate air from wood regions, pixels for porosity value below 0.95 were all inside wood region. It is clear that the porosity varies in a range from 0.4 to 0.7 for the wood samples, as shown in Fig. 2(a). There is a meniscus shaped dense region with porosity value below 0.4 on the up part of the sample, and actually it was the wood skin. Apparently, relatively large and low porosity, representing the sparse region with larger pore structure and/or a large number of small pores, and dense region with very small pore structure and/or very a few of small pores, distribute alternatively inside the wood sample, which is well consistent with normal pore distribution of a typical wood, ring-porous hardwood available in reference [18].

3.2. Saturation evolution

Fig. 3 illustrates the scanned images at different times during wetting course, or at 0 (dry wood), wetted 4, 8 and 32 h. Darker regions in an image, where grey scale decreases, indicate the places where water accumulated. Very clearly, water migrated from the outside to the center during wetting, and the wetting front was very clear and shrank towards the center, characterized by the dotted lines. Outside the wetting front the grey scale varied significantly, indicating much water transferred into this region. Inside the wetting front or center region little change occurred compared with the dry sample in Fig. 3(a), and it is difficult to identify whether water migrated in or not. A series of comparisons was conducted to explore the grey scale change or water migration on the referred line for a specified cross-section at different times in the wood sample, as well as corresponding porosity and saturation evolutions calculated using Eqs. (1) and (2).

Fig. 4(a) illustrates saturation and porosity distributions at wetted 4 h. The porosity fluctuates from 0.4 to 0.8 along the specified line, indicating the complex inner pore structure distribution. Crests and troughs of porosity illustrate the alternate distribution of sparse and dense inner pore structures. From the saturation curve, two different zones are distinguished by the dashed lines as the funicular ($S \geqslant S_{irr}$) and pendular ($0 \leqslant S \leqslant S_{irr}$) ones, assuming the irreducible saturation $S_{irr} = 0.4$ for normal wood materials [19],

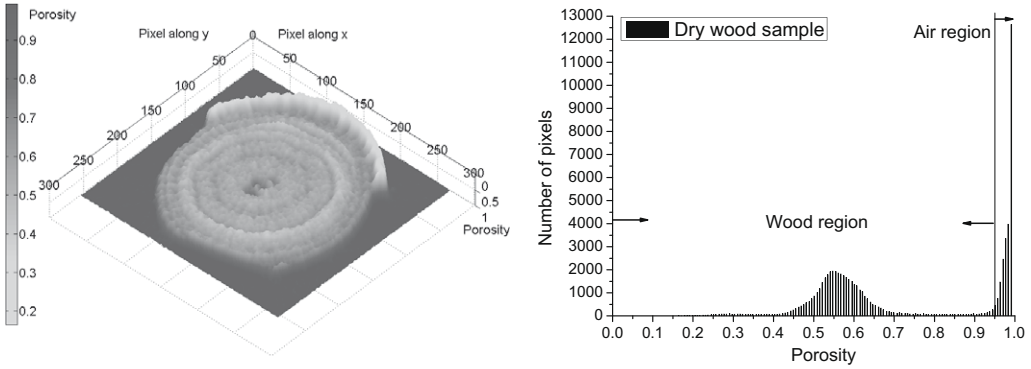

(a) Porosity distribution (b) Porosity histogram

Fig. 2. Porosity and corresponding histogram.

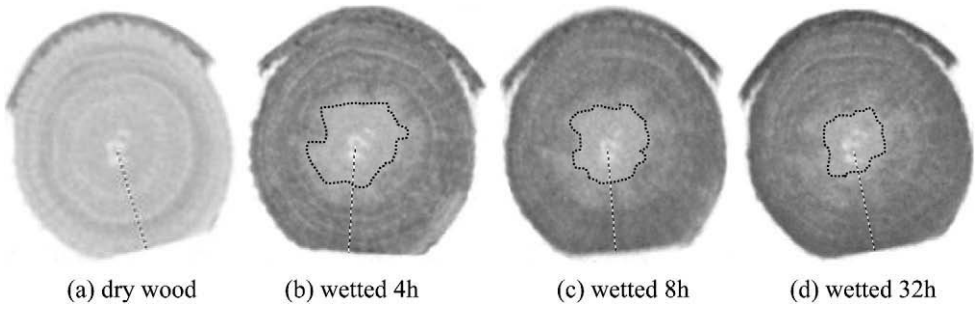

(a) dry wood (b) wetted 4h (c) wetted 8h (d) wetted 32h

Fig. 3. Images at different times during wetting.

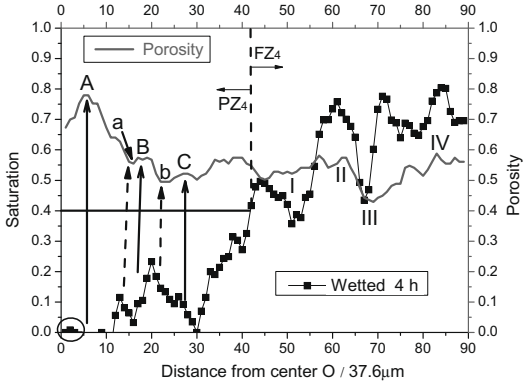

(a) Saturation at 4h

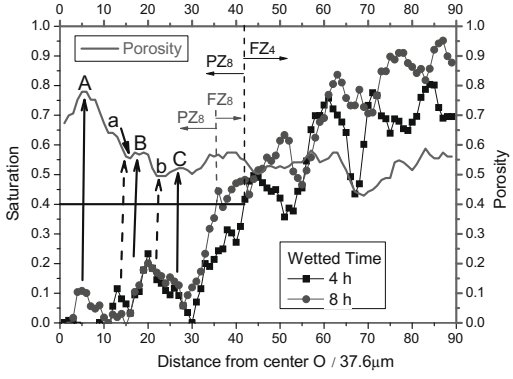

(b) Saturation at 4h and 8h

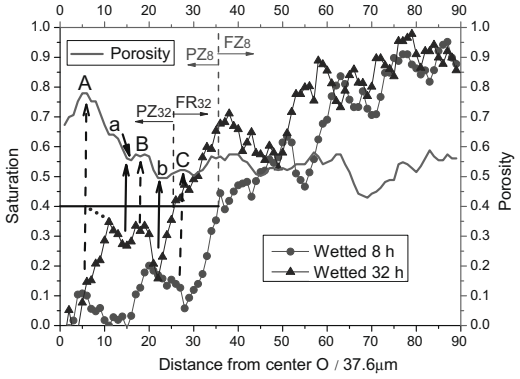

(c) Saturation at 8h and 32h

Fig. 4. Saturation evolution during wetting process.

above which free water would remain continuous, and below which free water would be discontinuous. FZ_4 and PZ_4 in Fig. 4(a) represent funicular and pendular zones for the wood sample after wetted 4 h, respectively. In FZ_4, due to the large and small porosity alternately distributes in the wood sample, the saturation distribution was not uniform, and these crests and troughs corresponding to large and small saturation. In PZ_4, A, B and C are the sparse regions having different maximum extrema of porosity, and among them both a and b are the dense regions with local minimum porosity values. Very clearly, during this earlier migration, water would easily absorbed and accumulated in relative denser regions rather than sparse ones, forming saturation crests in dense regions (a and b) and saturation troughs in sparse regions (A, B and C), as indicated by the arrows in Fig. 4(a) (solid arrows for dense regions and dashed arrows for sparse regions). It is expected that these phenomena were induced by the stronger capillary force in relatively denser regions. The saturation in "region a" is smaller than in "region b", indicating that water would first accumulate into b and then a through sparse region B during water migration from the outside to the center, and this can be considered as the first stage of the water wetting course. These local saturation crests and troughs are closely dependent upon the inner pore structure/size or the sparse and dense regions.

As depicted in Fig. 4(b), after wetted for 8 h water further accumulated and saturation increased in the sample. The boundary between funicular and pendular zones moved towards the center. In FZ_8, saturation mainly increased in the saturation trough regions at wetted 4 h and little alternation occurred in the crest regions, which makes the saturation crests and troughs at wetted 4 h reversed at wetted 8 h. In PZ_8, saturation was obviously increased in the sparse regions, A, B and C. However, in the dense regions, saturation was kept invariant or without more water accumulated, like "region b", and even decreased in "region a". Very clearly, after water was first transferred into the dense regions and further migrated inside the wood sample, water began accumulating in the sparse regions. This is the second stage of wetting.

The saturation distributions are presented in Fig. 4(c) for 8 and 32 h wetting. As water continually penetrated inside the wood, the pendular zone had a further shrinkage towards the center. In FZ_{32}, the saturation mainly increased in the saturation trough regions at wetted 8 h and little variation or even decrease occurred in the crest regions. The crests and troughs also reversed at wetted 32 h compared with those at wetted 8 h. Since large amount of water was transferred inside the zone PZ_{32}, the saturation increased significantly in both the sparse and dense regions, and the sparse region C even came into the funicular zone. The sparse regions of B and C had a greater saturation than the dense regions of a and b. According to this trend, the saturation distribution in the sparse region A should be expected as the dotted line in Fig. 4(c). However, the distribution was actually opposite. At this moment the water was still migrating into the center and the saturation would increase to approach the dot line finally. This is the third stage of wetting.

Look back to the regions I–IV in the zone FZ_4, far from the center. The regularity of saturation distribution is similar to that in the regions A, B, C, a and b in Fig. 4(c), with higher saturation in the relatively sparse regions II and IV and lower saturation in the relatively dense regions I and III. It is expected that the saturation distribution in zone FZ_4 had already experienced the first three stages of pendular mode and just reached funicular mode. So, as much more water came in, saturation in dense and sparse regions began to increase alternately with crests and troughs reversed variation, which can be clearly seen in the funicular zones of FZ_8 and FZ_{32} in Fig. 4(b) and (c). If the porosity in this wood sample distributed uniformly without dense and sparse regions, saturation would increase monotonously from outside to inside in funicular zone without fluctuation with crests and troughs, which has been demonstrated by the available experiments [20]. Consequently, the alternate variation of saturation crests and troughs was induced by complex distribution of dense and sparse regions.

Actually, above discussions were demonstrated by a series of experimental tests for different wood samples. Due to the space limit, no more results are presented here.

3.3. Inner structural effects

Summarizing the transport characteristics discussed above, it can be concluded that water transfer and accumulation in funicular and pendular zones had distinct features, and the saturation evolution characteristics are expected to be induced by different water transport modes existing in different stages during the wetting process. Accordingly, it is crucial to clarify transport modes and each effect on the liquid migration. Fig. 5 illustrates ideal models of four general transport modes for water inside porous structures, entrapped in narrow slits, spread on pore surface, continuous flow and phase change transport. At wetting beginning and/or very low saturation, it is hard to form continuous flow inside the pore structures. Normally water would mainly be entrapped in narrow slits easily and stay steadily or spread in these slits as a result of capillary force, or form droplets and spread on pore surface and even to a thin film in relatively large pore structures, as shown in Fig. 5(a) and (b). The entrapping and spreading behavior are expected to be triggered and highly influenced by the inner geometrical structure, as well as the wetting performance between solid and liquid. These modes likely occur in pendular zone or for pendular mode. When wetting continues and saturation increases, continuous flow is formed, as shown in Fig. 5(c). Water is entrapped in all narrow slits and covers almost all of pore surfaces, and effects induced by inner structure and pore surface performance are decayed or even disappeared. Consequently, liquid transport is mainly influenced by local saturation variation. In case undergoing phase change inside porous media, such as evaporation and condensation, another transport mode of liquid will emerge, as shown in Fig. 5(d). Due to the gas/vapor–liquid interface shape and contact between solid and liquid determined by complex surface topography, the performance of phase change transport phenomena is also highly influenced by inner geometric structure. These ideal transport models might be helpful to understand and/or explain the present experimental observations.

During wetting process, three modes, as shown in Fig. 5(a), (b) and (c), were observed, and different effects were motivated on water transport phenomena and corresponding saturation evolution characteristics. In pendular mode, water first penetrated into dense regions in Fig. 4(a) and accumulated in narrow slits because of great capillary force, as shown in Fig. 5(a). As a further migration into the inside, water began accumulating in the sparse regions as shown in Fig. 4(b) and was expected to spread on relatively smooth pore surface, as shown in Fig. 5(b). Meanwhile, in the dense regions the saturation was invariant or even decreased. It is concluded that for pendular mode evolution of the saturation or water migration had an intimate relation with pore scale, local distribution of dense or sparse regions, pore geometric structure and wall surface, since existence of the dynamical contact of liquid–air/vapor interface with solid surface having complex surface topography and corresponding form of water in the pore structure of the sample were dependent of all these factors. Finally, due to much water transferred in the sample, water further assembled in both sparse and dense regions, and saturation in sparse regions was greater than that in dense regions, as shown in Fig. 4(c). At this moment, some sparse regions changed the original pendular mode to funicular mode. In funicular mode, water transferred inside the sample with periodical alternation of the saturation crests and troughs during

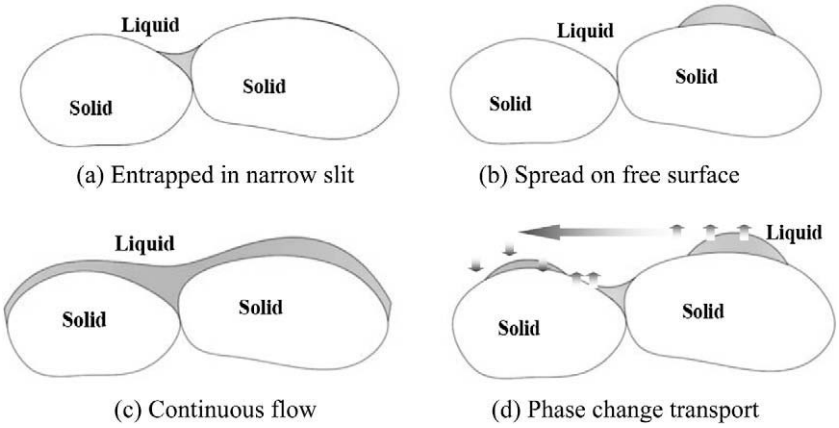

Fig. 5. Transport modes in porous media.

wetting process, indicating highly non-uniform of the transport. Local distribution of dense and sparse regions and pore scale seemed to have influence on the transport in this region, while both pore structure and pore surface performance did not affect the water migration, since water had already filled with all slit structures and covered all pore wall surfaces and there was no contact of liquid–air interface with solid, as shown in Fig. 5(c).

Furthermore, it was surprised to observe saturation variation quite in the center as shown by the circle in Fig. 4(a). Since the surrounding saturation was kept zero, it is expected that the water was transferred into this region by evaporation and condensation, as shown in Fig. 5(d), which was mainly induced by variations of humidity and saturated vapor pressure in the air phase during wetting.

4. Conclusions

In present work, both saturation evolution and corresponding liquid transfer in pore structures of porous media are investigated nondestructively for both pendular and funicular modes during wetting processes using the micro CT. A novel method was developed to obtain the important real inner information of porous media, such as pore diameter distribution, local porosity, as well as saturation profile and evolution, and corresponding liquid migration. During the whole wetting process, the pendular and funicular mode could be identified distinctly by irreducible saturation, and for each mode the characteristics of transport process were explored based on local pore structural information. For pendular mode, water first accumulated into the dense regions and little in sparse regions. Then due to further wetting, water began migrating in the sparse regions and saturation in dense regions was kept invariant or without more water accumulated. Finally, since large amount of water was transferred inside, the saturation increased significantly in both the sparse and dense regions, and some sparse regions became the funicular zone. For funicular mode, due to the large and small porosity alternately distributes in the wood sample, the saturation distribution was not as uniform as that during wetting in homogenous porous media. The local saturation crests and troughs, corresponding to large and small saturation, existed and varied alternately. It can be concluded that water transfer and accumulation in funicular and pendular zones had distinct features, and the saturation evolution characteristics are expected to be induced by different water transport modes existing in different stages during wetting. Particularly, for the pendular mode, existence of distinct accumulation states, such as assembling in a narrow slit, droplet or film on a pore wall surface, as well as their dynamical evolution and corresponding inner structure effects during wetting were further discussed and supply a deep understanding of present experimental observations.

Acknowledgement

This research is currently supported by the National Natural Science Foundation of China (No. 50636030).

References

[1] R. Lenormand, E. Touboul, C. Zarcone, Numerical models and experiments on immiscible displacement in porous media, J. Fluid Mech. 189 (1988) 165–187.
[2] D. Geromichalos, F. Mugele, S. Herminghaus, Nonlocal dynamics of spontaneous imbibition fronts, Phys. Rev. E 89 (10) (2002) 104503.
[3] H.O. Yidiz, M. Gokmen, Y. Cesur, Effect of shape factor, characteristic length and boundary conditions on spontaneous imbibition, J. Petrol. Sci. Eng. 53 (3–4) (2006) 158–170.
[4] E.W. Washburn, The dynamics of capillary flow, Phys. Rev. 17 (3) (1921) 273–283.
[5] L.L. Handy, Determination of effective capillary pressure for porous media from imbibition data, Trans. AIME 219 (1960) 75–80.
[6] D.A. Lockington, J.Y. Parlange, A new equation for macroscopic description of capillary rise in porous media, J. Colloid Interface Sci. 278 (2004) 404–409.
[7] G.A. Spolek, O.A. Plumb, Capillary pressure in softwoods, Wood Sci. Technol. 15 (1981) 189–199.
[8] M.J. Blunt, H. Scher, Pore-level modeling of wetting, Phys. Rev. E 52 (6) (1995) 6387–6403.
[9] G.N. Constantinides, A.C. Payatakes, Effects of precursor wetting films in immiscible displacement through porous media, Transport Porous Med. 38 (3) (2000) 291–317.
[10] S. Whitaker, W.T.H. Chou, Drying of granular porous media-theory and experiment, Dry. Technol. 1 (1) (1983–1984) 3–33.
[11] S. Whitaker, Moisture transport mechanisms during the drying of granular porous media, in: Proceedings of the Fourth International Drying Symposium, Kyoto (Japan), July 9–12, 1 (1984) 31–42.
[12] P. Perré, I.W. Turner, Transpore: a generic heat and mass transfer computational model for understanding and visualising the drying of porous media, Dry. Technol. 17 (7–8) (1999) 1273–1289.
[13] J.R. Puiggali, M. Quintard, Properties and simplifying assumptions for classical drying models, Adv. Dry. 5 (1992) 131–147.
[14] W.B. Lindquist, S. Lee, Medial axis analysis of void structure in three-dimensional tomographic images of porous media, J. Geophys. Res. 101 (B4) (1996) 8297–8310.
[15] W.B. Lindquist, A. Venkatarangan, Investigating 3D geometry of porous media from high resolution images, Phys. Chem. Earth A Solid Earth Geodesy 24 (7) (1999) 593–605.
[16] D. Wu, X.F. Peng, Investigation of water migration in porous material using micro-CT during wetting, Heat Transfer Asian Res. 36 (4) (2007) 198–207.
[17] D. Wu, X.F. Peng, Scanning analysis of water migration in wood using micro-CT during wetting and drying, The 19th International Symposium on Transport Phenomena August 17–20, 2008, p. 72.
[18] Structure of wood, Society of Wood Science and Technology, Teaching Unit No. 1, 2003, http://www.swst.org/teach/set2/struct1.html, Cited 16 June 2003.
[19] M. Goyeneche, D. Lasseux, D. Bruneau, A film-flow model to describe free water transport during drying of a hygroscopic capillary porous medium, Transport Porous Med. 48 (2) (2002) 125–158.
[20] S. Roels, J. Carmeliet, Analysis of moisture flow in porous materials using microfocus X-ray radiography, Int. J. Heat Mass Transfer 49 (25–26) (2006) 4762–4772.